

Fermi Surface Reconstruction in CeTe₂ Induced by Charge Density Wave: ARPES Study

J.-S. Kang¹, D. H. Kim¹, H. J. Lee¹, J. H. Hwang¹, Han-Koo Lee², H.-D. Kim²,
B. H. Min³, K. E. Lee³, Y. S. Kwon³, J. W. Kim⁴, Kyoo Kim⁴, B. H. Kim⁴, and B. I. Min⁴

¹Department of Physics, The Catholic University of Korea, Bucheon 420-743, Korea

²Pohang Accelerator Laboratory, POSTECH, Pohang 790-784, Korea

³Department of Physics, Sungkyunkwan University, Suwon 440-746, Korea and

⁴Department of Physics, Pohang University of Science and Technology, Pohang 790-784, Korea

(Dated: February 5, 2022)

Electronic structures of a charge-density-wave (CDW) system CeTe_{2-x}Sb_x ($x=0, 0.05$) have been investigated by employing angle-resolved photoemission spectroscopy (ARPES). The observed Fermi surface (FS) agrees very well with the calculated FS for the undistorted CeTe₂ both in shapes and sizes. The metallic states crossing the Fermi level (E_F) are observed in ARPES. The carriers near E_F have mainly the Te(1) $5p$ character, with the negligible contribution from Ce $4f$ states to the CDW formation. The supercell (shadow) bands and the corresponding very weak FS's are found to arise from band-folding due to the interaction with Ce-Te(2) layers. This work shows that the origin of the CDW formation in CeTe₂ is the FS nesting and that the CDW modulation vector is along Γ -X ($\mathbf{Q}_{CDW} \approx \mathbf{X}$).

PACS numbers: 79.60.-i, 71.45.Lr, 71.18.+y, 71.20.-b

The charge-density-wave (CDW) formation is one of the most interesting phenomena in solid state physics.[1–3] CeTe₂ is known as a CDW system having a high CDW transition temperature of $T_{CDW} \sim 1000$ K, and the CDW state in CeTe₂ coexists with magnetism and also with superconductivity ($T_C = 2.7$ K) under pressure.[4] CeTe₂ crystallizes in the quasi-two dimensional layered Cu₂Sb-type tetragonal structure with two types of Te sites: Te(1) and Te(2). Te(1) atoms form planar square sheets, which are sandwiched along the c axis by the corrugated double layers of Ce and Te(2) atoms (Fig. 1). The ionic configuration of CeTe₂ is considered to be Ce³⁺Te(2)²⁻Te(1)¹⁻, so that hole carriers are produced in Te(1) sheets.[5] Then the square net of Te(1) would be easily distorted by the Peierls-like mechanism[6] due to the partial filling. Underneath this picture is the assumption of trivalent Ce³⁺ states.[7] Band-structure calculations indicate that the CDW instability occurs due to the nesting between the Fermi surfaces in Te(1) square sheets in the ab plane,[8–10] which was supported experimentally.[11]

Due to the difficulty in growing high-quality single crystals for the angle-resolved photoemission spectroscopy (ARPES) study, there have been only a few ARPES studies of CeTe₂. A couple of works reported the Fermi surface (FS) topology in the CDW state of CeTe₂, as well as that in a similar CDW system LaTe₂, by using ARPES.[12–14] Shin *et al.*[12] reported that the FS topology of CeTe₂ in the k_x - k_y plane is different from that of LaTe₂. [13] The small square FS centered around Γ , predicted by band calculations, was not observed in ARPES. So they conjectured that the CDW gap E_g is larger than ≥ 600 meV, and that the magnitude of E_g varies around the FS. This minimum value

of $E_g \approx 600$ meV is much larger than $E_g \approx 100$ meV, found in another ARPES study.[5] The CDW distortion probed by TEM[12] was somewhat different from that in the literature,[11] which was attributed to the variation of the Te deficiency produced by different sample growth techniques. Ito *et al.*[14] examined the FS along the k_z axis, and observed a systematic intensity modulation in the spectral weight at FS.

The natural question is whether the FS topology and the CDW state of CeTe₂ are similar to those of LaTe₂ or not. This includes the following issues: (i) do the FS and the CDW distorted structure in CeTe₂ have the same symmetry as those in LaTe₂?, (ii) how large is the effect

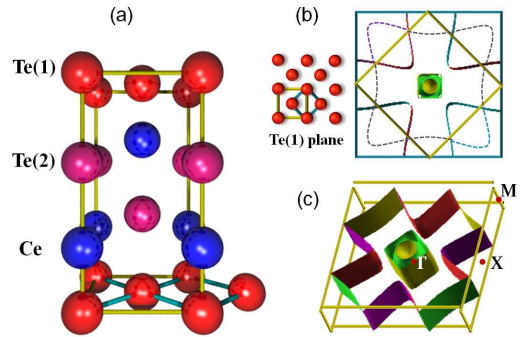


FIG. 1: (Color online) (a) Tetragonal crystal structure of CeTe₂ in the non-CDW phase. The unit cell of Te(1) square net is doubled in tetragonal CeTe₂. (b) The Brillouin Zone (BZ) of Te(1) sheets (outer square) is reduced to half (inner square) because of the larger cell size of Ce-Te(2) layers. (c) Fermi surface of CeTe₂ in the tetragonal BZ of the non-CDW phase, corresponding to the inner square in (b).[15] Γ , X, and M represent $\mathbf{k}=(0, 0, 0)$, $\frac{2\pi}{a}(1/2, 0, 0)$, and $\frac{2\pi}{a}(1/2, 1/2, 0)$, respectively.

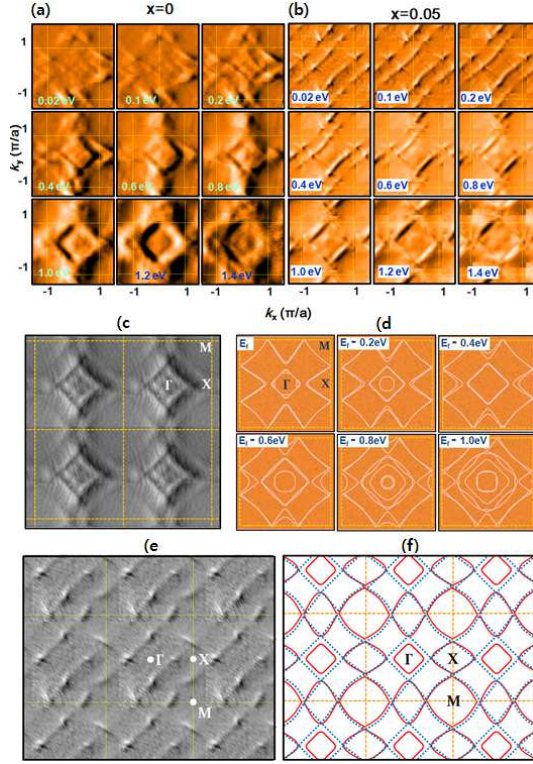


FIG. 2: (Color online) (a) First derivatives of the constant-energy (CE) map of CeTe_2 with the increasing binding energy (BE) between $\text{BE}=0.02$ eV and $\text{BE} \sim 1.4$ eV. (b) Similarly for $\text{CeTe}_{1.95}\text{Sb}_{0.05}$. Here $\text{BE}=|E_i|$, where E_i denotes the initial-state energy. Dotted lines denote the BZ. (c) The experimental CE map of CeTe_2 for $\text{BE}=1.0$ eV, drawn in the periodic zone scheme. This map was generated by the reflections of the map data that were obtained for a smaller region of the BZ. (d) The calculated CE map of CeTe_2 as a function of E_i . (e) The experimental FS map of $\text{CeTe}_{1.95}\text{Sb}_{0.05}$. (f) Comparison of the experimental FS map (blue dotted lines) and calculated FS map (red solid lines).

of the band folding, due to the interaction between $\text{Te}(1)$ and $\text{Ce-Te}(2)$ layers, on the FS of $\text{Te}(1)$ sheets?, and (iii) what is the CDW modulation vector, \mathbf{Q}_{CDW} ? As shown in Fig. 1(b), the Brillouin Zone (BZ) of $\text{Te}(1)$ sheets is reduced to half, and thereby, the bands are folded into the reduced BZ to yield the supercell (shadow) bands. The FS's, denoted with dotted lines in Fig. 1(b), come from those shadow bands. We have resolved these questions by performing careful ARPES measurements for high-quality stoichiometric single crystals of $\text{CeTe}_{2-x}\text{Sb}_x$ ($x = 0, 0.05$). We also report the detailed study of the FS topology, the energy-dependent behavior of the constant energy (CE) map, and the clearly dispersive feature of the states near the Fermi level (E_F) in CeTe_2 .

High-quality $\text{CeTe}_{2-x}\text{Sb}_x$ single crystals having very low residual resistivity were grown by using the self-fluxed Bridgman method.[16] The quality and the orientation of the single crystal were checked by Laue patterns.

ARPES experiments were carried out at the 3A1 beam-line of the Pohang Light Source (PLS) with the beam size of $< 50 \mu\text{m}$ and using a Scienta SES-2002 electron energy analyzer. Single crystals were cleaved *in situ* at $T \sim 30$ K under the pressure better than 5×10^{-11} Torr, which exposed the (001) surfaces. The Fermi level and the overall instrumental resolution of the system were determined from the Fermi edge of an evaporated Cu metal. The energy resolution (ΔE) and the momentum resolution (Δk) were set to be $\Delta E \sim 80$ meV and $\Delta k \approx 0.01 \text{\AA}^{-1}$, respectively, at $h\nu \sim 110$ eV.

Figure 2 shows the first derivatives of the CE maps of CeTe_2 (Left) and $\text{CeTe}_{1.95}\text{Sb}_{0.05}$ (Right) vs. the initial-state energy (E_i) of $-1.4 \text{ eV} \leq E_i \leq -0.02 \text{ eV}$. These data were obtained at $T \sim 30$ K with $h\nu \approx 115$ eV. In plotting each CE map, the spectral intensity of $E_i \pm 100$ meV was integrated. This figure shows that the CE maps of $x=0$ and $x=0.05$ are essentially the same in their shapes, sizes, and energy-dependent behavior. But the CE maps of $x=0.05$ are sharper than those of $x=0$. Thus the energy-dependent evolution of the CE map is manifested more clearly in $x=0.05$ than in $x=0$. [17]

The four-fold symmetry is observed in the FS[18] and CE maps for both $x=0$ and 0.05 . The feature of the four-fold symmetry is shown more clearly in the CE map for $E_i = -1.0$ eV (Fig. 2(c)), which was obtained from a different cleave. Two diamond-shaped contours are observed in the FS map, which is similar to the case of LaTe_2 . [13] This finding implies that Ce $4f$ electrons hardly contribute to the states near E_F . Note that the inner-diamond FS is clearly seen in both $x=0$ and 0.05 , in contrast to the case of Ref.[12]. With increasing $|E_i|$, the size of the inner diamond increases, while that of the outer diamond remains nearly the same. Such an energy-dependent behavior is consistent with that of the calculated FS's, shown in Fig. 2(d).

Figure 2(e) shows the FS of $\text{CeTe}_{1.95}\text{Sb}_{0.05}$, drawn in the periodic zone scheme. This FS map was obtained by integrating the ARPES spectra for $E_F \pm 50$ meV ($E_F \equiv 0$ eV). The existence of the FS implies that there remain metallic states even below the CDW transition, producing the remnant ungapped FS. This conclusion is supported by the calculated FS, shown in Fig. 2(f). In Fig. 2(f), the experimental FS is compared with the calculated FS. The former is obtained by interpolating the partially ungapped FS's and the latter is calculated for the non-CDW phase.[10] The experimental and calculated FS's are very similar to each other in both sizes and shapes, supporting that the measured FS reflects the FS of the non-CDW phase of CeTe_2 . Two important features are noted here. First, this comparison confirms the FS nesting mechanism for the CDW formation in CeTe_2 . Secondly, the opening of the CDW gaps occurs only partially in some part of the FS, which is consistent with the semimetallic nature of CeTe_2 . [5, 19, 20]

According to band calculations, there are two FS

nesting vectors, one parallel to Γ -X ($\mathbf{Q}_1 \approx \mathbf{X}$), and the other parallel to Γ -M ($\mathbf{Q}_2 \approx \mathbf{M}/2$) for both LaTe_2 [8] and CeTe_2 . [10] In general, \mathbf{Q}_{CDW} is determined by the FS nesting vector.[9] In real systems, however, the CDW transition occurs only when there exists a soft phonon mode at a specific \mathbf{Q}_{CDW} . In order to check the existence of a soft phonon mode in CeTe_2 , we have calculated the phonon dispersion $\omega(\mathbf{q})$ for LaTe_2 for simplicity.[21] Indeed, the calculated $\omega(\mathbf{q})$ (Fig. 3) exhibits negative values near X. This finding manifests phonon softening at $\mathbf{Q}_1 \approx \mathbf{X}$, and suggests that \mathbf{Q}_{CDW} in CeTe_2 corresponds to $\mathbf{Q}_1 \approx \mathbf{X}$, but not to $\mathbf{Q}_2 \approx \mathbf{M}/2$.

In Fig. 4, we have compared the ARPES intensity plots of CeTe_2 with the band structures, calculated for the non-CDW lattice.[15] Left sides of Fig. 4(a) and (b) show the ARPES data of CeTe_2 along Γ -M in two different paths, along A and along D, respectively, as shown in Fig. 4(c). ARPES intensity plots were made by taking second derivatives of the ARPES data, obtained with $h\nu \approx 104$ eV. The experimental band structures of $\text{CeTe}_{1.95}\text{Sb}_{0.05}$ (not shown here) are found to be essentially the same as those of CeTe_2 without a noticeable energy shift within the instrumental resolution.[17] Many dispersive bands, observed clearly in ARPES, indicate the good quality of the samples employed in this study. The overall band structures of Fig. 4(a) and (b) are similar to each other.

But there are also some differences between two, which seem to arise from (i) the band-folding effect due to the increased unit cell (see Fig. 1(b)), and (ii) differences in the topography of the cleaved surfaces.[22] The band-folding effect is clearly seen in the calculated band structures, shown on the right sides of Fig. 4(a) and (b). For the calculated band structure and FS, the band unfolding scheme[23] is adopted to separate out the shadow bands and the corresponding FS in the larger BZ from the non-shadow (main) bands and the corresponding FS. In this scheme, the intensity of the $\text{Te}(1)$ supercell band is proportional to the interaction between the $\text{Te}(1)$ layer and the underlying $\text{Ce-Te}(2)$ layer. If the interaction is weak,

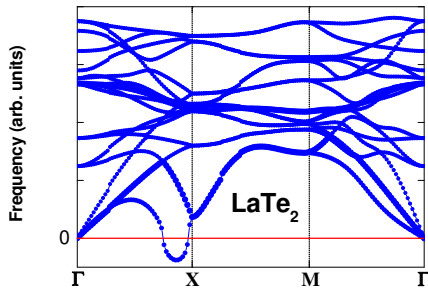


FIG. 3: (Color online) Phonon dispersion $\omega(\mathbf{q})$ of undistorted LaTe_2 . Negative $\omega(\mathbf{q})$ here represents the imaginary part of the phonon frequency. Phonon softening occurs at $\mathbf{Q}_1 \approx \mathbf{X}$ ($\omega^2(\mathbf{Q}_1) < 0$).

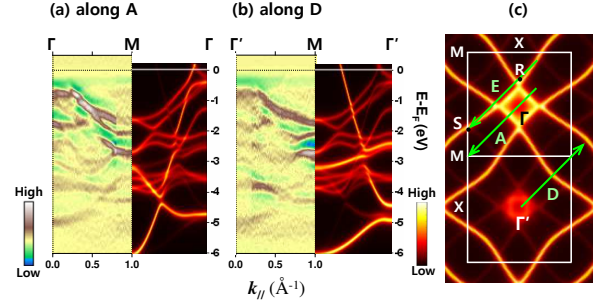


FIG. 4: (Color online) (a) ARPES along A (Γ -M), with the calculated band structures along Γ -M on the right, which is attached as a mirror image. (b) Similarly for along D (Γ -M). (c) Unfolded FS in the extended BZ, where two different Γ -M paths, *i.e.* along A and D, are indicated. Note that the shadow bands and the corresponding FS are barely seen.

it results in the weakening of weights of supercell-folded bands and the corresponding FS. In Fig. 4(a), the wide in-plane $\text{Te}(1)$ $5p$ band[10] starting from M at ~ -6.2 eV to near Γ ($\sim 0.2M$) at E_F is prominent, while in Fig. 4(b), the in-plane $\text{Te}(1)$ $5p$ band starting from Γ' at ~ -4.5 eV to near M ($\sim 0.7M$) at E_F is prominent. In fact, the latter is seen as a dim shadow band in Fig. 4(a), and vice versa in Fig. 4(b). The main and shadow bands in Fig. 4(a) produce the bright inner FS and the dim outer FS in the first BZ, respectively, shown in the top BZ of Fig. 4(c).

A very good agreement is found between ARPES and calculation in both the dispersive feature and the energy positions of the bands below -0.6 eV. However, some discrepancies are also observed. Some of the calculated bands are missing in ARPES. In particular, the E_F -crossing bands near Γ and M in theory, originating from $\text{Te}(1)$ $5p$ -states, are not observed clearly in ARPES. Only the dim features are barely seen in Fig. 4(a) and (b). In order to see the bands near E_F more clearly, the ARPES intensity plots in the vicinity of E_F are shown in Fig. 5. Figures 5(a), (b), and (c) show the near- E_F raw ARPES spectra of $\text{CeTe}_{1.95}\text{Sb}_{0.05}$ along E and those of CeTe_2 along A and D in the BZ, respectively. Figure 5(d) shows the stack of momentum distribution curves (MDC's), corresponding to the constant-energy cuts through the ARPES intensity plots shown in Fig. 5(c).

The band-crossing through E_F is clearly observed in Fig. 5(a). These states are expected to produce the FS's at the corresponding \mathbf{k}_F values.[24] On the other hand, in Fig. 5(b) and (c), there are bands approaching E_F , but their spectral intensities die away as they approach E_F . The expected E_F -crossing positions in ARPES agree very well with those in the calculated bands for the non-CDW phase of CeTe_2 (see Fig. 4), which have mainly $\text{Te}(1)$ $5p$ character.[10] As shown in Fig. 4(c), two bands near Γ ($\sim 0.2M$) and M ($\sim 0.7M$) in Fig. 5(b) would produce

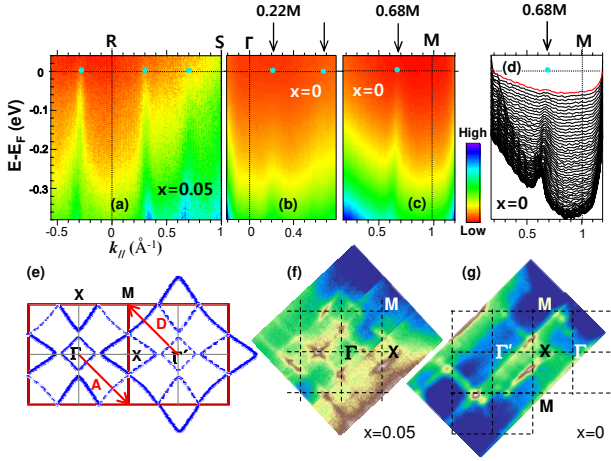


FIG. 5: (Color online) (a) Near- E_F ARPES intensity plots of $\text{CeTe}_{1.95}\text{Sb}_{0.05}$ along E (see Fig. 4(c)). (b) Near- E_F ARPES of CeTe_2 along A (Γ -M) in the first BZ. (c) Near- E_F ARPES of CeTe_2 along D (Γ' -M) in the second BZ. (d) Stack of MDC's, corresponding to $E_i = 0$ (E_F) and $E_i = -0.4$ eV, respectively. (e) Calculated FS maps for the non-CDW state of CeTe_2 . Dotted lines represent the folded FS's. (f) Experimental FS map of $\text{CeTe}_{1.95}\text{Sb}_{0.05}$. (g) Similarly for CeTe_2 . In (f) and (g), Γ and Γ' denote the Γ points in the first BZ and the second BZ, respectively.

the inner (bright) FS and outer (dim) FS's along Γ -M in the first BZ, respectively. Similarly, the band near M ($\sim 0.7M$) in Fig. 5(c) would produce the larger FS along Γ -M in the second BZ. The much weaker spectral weight of the band near M in Fig. 5(b), as compared to that near Γ , is attributed to its nature of the shadow band, which originates from the band-folding.

The vanishing spectral intensity near E_F in Fig. 5 is considered to be related to the opening of the CDW gaps in some part of the FS's. This feature is revealed more clearly in Fig. 5(f) and 5(g), which show the experimental FS maps of the first BZ and the second BZ, respectively, obtained by integrating $E_F \pm 100$ meV. These are not the derivative data, but raw data. The inner FS near Γ is certainly observed in Fig. 5(f), while the outer diamond FS is very weak. In contrast, the inner diamond FS near Γ' is hardly seen in Fig. 5(g) but the outer diamond FS is apparent. In view of the calculated FS's in Fig. 4(c) and Fig. 5(e), such differences can be interpreted as the fact that the FS's in Fig. 5(f) correspond to those in the first BZ, whereas the FS in Fig. 5(g) corresponds to that in the second BZ.

The feature of the vanishing spectral weight is also observed in some part of the FS's: for example, in Fig. 5(f), the spectral weight near M is almost vanishing, and the outer diamond FS shows an intermittent feature. The polarization effect is not likely the origin of an intermittent feature of the outer FS since this feature is common

for all four sides of the outer diamond. Instead, this region would correspond to the \mathbf{k} -points where CDW gaps open. Therefore the diminishing feature in Fig. 5(b) and (c) reflects the opening of the CDW gap. One can estimate the size of the CDW energy gap as being $E_g \simeq 50$ meV near M, in agreement with our previous finding in a different ARPES study.[5]

In conclusion, the FS measured by ARPES agrees very well with the calculated FS for the undistorted CeTe_2 both in shapes and sizes, and the E_F -crossing metallic states are clearly observed in ARPES. We have found the following answers to the questions addressed in the beginning: (i) The measured FS is similar to that of LaTe_2 , implying that Ce 4*f* states have a minor contribution to the CDW formation in CeTe_2 . (ii) The band-folding originating from the interaction with Ce-Te(2) layers produces the shadow bands and the corresponding FS's, which have very weak spectral weight. (iii) The CDW modulation vector is estimated to be $\mathbf{Q}_{CDW} = \mathbf{Q}_1 \approx \mathbf{X}$.

This work was supported by the NRF under Contract No. 2009-0064246 and No. 2009-0079947. YSK acknowledges the NRF grant under Contract No. 2006-2002165 and 2009-0078025. PLS is supported by POSTECH and MEST in Korea.

-
- [1] J. Voit, *et al.*, Science **290**, 501 (2000).
 - [2] T. Kasuya, M. H. Jung, and T. Takabatake, J. Magn. Magn. Mater. **220**, 235 (2000).
 - [3] T. Yokoya, *et al.*, Science **294**, 2518 (2001).
 - [4] M. H. Jung, *et al.*, Phys. Rev. B **67**, 212504 (2003).
 - [5] J.-S. Kang, *et al.*, Phys. Rev. B **74**, 085115 (2006).
 - [6] J. K. Burdett and S. Lee, J. Amer. Chem. Soc. **105**, 1079 (1983).
 - [7] J.-S. Kang, *et al.*, J. Phys.: Condens. Matter **16**, 9163 (2004).
 - [8] A. Kikuchi, J. Phys. Soc. Jpn. **67**, 1308 (1998).
 - [9] E. DiMasi, *et al.*, Phys. Rev. B **54**, 13587 (1996).
 - [10] J. H. Shim, J.-S. Kang, and B. I. Min, Phys. Rev. Lett. **93**, 156406 (2004).
 - [11] K. Stöwe, J. Alloy Compd. **307**, 101 (2000).
 - [12] K. Y. Shin, *et al.*, Phys. Rev. B **72**, 085132 (2005).
 - [13] D. R. Garcia, *et al.*, Phys. Rev. Lett. **98**, 166403 (2007).
 - [14] T. Ito, *et al.*, J. Magn. Magn. Mater. **310**, 431 (2007).
 - [15] We have employed the FLAPW band method in the LSDA+*U*+SO scheme. H. J. F. Jansen, A. J. Freeman, Phys. Rev. B **30**, 561 (1984); P. Blaha *et al.*, WIEN2k (ISBN 3-9501031-1-1), Karlheinz Schwarz, Techn. Universität Wien, Austria (2001).
 - [16] B. H. Min, H. Y. Choi, and Y. S. Kwon, Physica B **312-313**, 203 (2002); *ibid* **312-313**, 205 (2002).
 - [17] The ground state and the electronic structures of CeTe_2 remain almost the same in $\text{CeTe}_{1.95}\text{Sb}_{0.05}$ in this energy scale since the Sb-concentration in $\text{CeTe}_{1.95}\text{Sb}_{0.05}$ is very low (2.5%).
 - [18] The map with $E_i = -0.02$ eV can be regarded as the FS because $E_F \equiv 0$ is included in this map.
 - [19] M. Lavagnini, *et al.*, Phys. Rev. B **75**, 205133 (2007).

- [20] K. E. Lee, *et al.*, Phys. Rev. B **78**, 134408 (2008).
- [21] QUANTUM ESPRESSO code, Giannozzi, *et al.*, J. Phys. Condens. Matter **21**, 395502 (2009).
- [22] All the cleaved surfaces were mirror-shiny, but had many stepped planes. Due to a finite acceptance angle of the electron analyzer and a different topography of a cleaved surface, each cleaved surface is expected to have a different yield.
- [23] W. Ku, T. Berlijn, C.-C. Lee, Phys. Rev. Lett. **104**, 216401 (2010).
- [24] In the energy distribution curves (EDC's), the photoemission peaks that cross E_F were not observed clearly. Nevertheless, the E_F -crossing of these bands is supported by the slope of these bands.